

# A co-deployed dust-logging instrument for the IceCube Upgrade and IceCube-Gen2

## The IceCube Collaboration

(a complete list of authors can be found at the end of the proceedings)

*E-mail:* [anna.eimer@fau.de](mailto:anna.eimer@fau.de), [martin.rongen@fau.de](mailto:martin.rongen@fau.de)

A precise understanding of the optical properties of the instrumented Antarctic ice sheet is crucial to the performance of optical Cherenkov telescopes such as the IceCube Neutrino Observatory and its planned successor, IceCube-Gen2. One complication arising from the large envisioned footprint of IceCube-Gen2 is the larger impact of the so-called ice tilt. It describes the undulation of ice layers of constant optical properties within the detector.

In this contribution, we will describe the project to build a co-deployed laser dust logger. This is a device to measure the stratigraphy of impurities in the ice to derive the ice tilt. It consists of a light source that will be co-deployed with the photosensor modules, meaning it is part of the deployment string and operated during the deployment of the detector. The newly developed device will be tested during the deployment of the IceCube Upgrade in the 2025/26 austral summer to pave the way for IceCube-Gen2.

**Corresponding authors:** Anna Eimer<sup>1\*</sup>, Martin Rongen<sup>1</sup>

<sup>1</sup> *Erlangen Centre for Astroparticle Physics (ECAP), Friedrich-Alexander-Universität Erlangen-Nürnberg*

\* Presenter

39th International Cosmic Ray Conference (ICRC2025)  
15–24 July 2025  
Geneva, Switzerland



## 1. Ice stratigraphy

The IceCube Neutrino Observatory [1] is a cubic kilometer array of photosensors in the ice at the South Pole, detecting neutrinos. Neutrino interactions produce charged secondary particles that produce Cherenkov light. Since this Cherenkov light might get absorbed or scattered on its way from its origin in the ice to the detector module, it is crucial to know the optical properties of the ice for the reconstruction of neutrino properties from raw data.

Due to the ice formation over thousands of years and different dust concentrations in the air at different times, ice with similar optical properties is arranged in layers [2]. These layers are deposited at the same time and thus have the same optical properties. Therefore, they are called isochrones. Looking at the isochrones over the whole depth of the ice gives the ‘ice stratigraphy’. Certain features make it possible to relate the ice at a certain depth to known geological events in time, e.g. volcanic eruptions [2] (visible as very narrow highly scattering layers) or global features like the ‘dust layer’ with a high scattering coefficient over a larger depth range [2].

One way of measuring the scattering of light in ice is the ‘laser-based dust logging’ [2]. This device shines laser light horizontally into the ice. The light will then be scattered in the ice layer and a fraction scatters back to the instrument. An integrated photomultiplier tube (PMT) finally collects the scattered light. This principle is used over the whole depth of the IceCube detector. The result of these measurements for IceCube are shown in Figure 1. The signal strength is proportional to the amount of impurities in the ice.

Additionally, these layers of optical properties are not flat over the full detector volume. The layers follow the shape of the bedrock beneath the glacier and flatten out towards the surface. These undulations, called ‘tilt’ in IceCube, can be measured by logging the stratigraphy at different position within the instrumented ice. This was already done for IceCube with eight laser-based dust-logger measurements [2]. Those measurements needed a separate deployment immediately after drilling the hole, as well as a retrieval before the photosensors can be lowered. Therefore, this procedure was very time-consuming. Since then, several other methods were explored to measure the tilt. The currently used method in the IceCube ice model reconstructs the tilt with flasher LEDs incorporated in the IceCube digital optical modules (short DOMs) [3]. Most recently, camera data

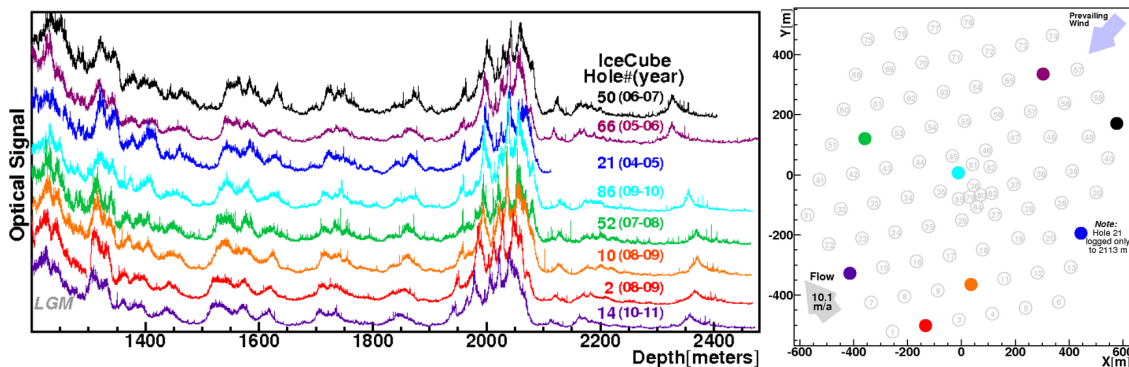


**Figure 1:** Stratigraphy measurements performed for IceCube. The left plot shows the optical signal in arbitrary units over the depth in meter. The colors in this plot correspond to the color coded positions in the detector layout on the right. (Taken from [2])

was used for a feasibility study to measure the ice stratigraphy [4].

The tilt measurement will be crucial for the larger footprint and larger module spacing envisioned for IceCube-Gen2 [5]. Hence, a more practical version of the ‘dust logger’, called the LOMlogger, will be tested in the low energy extension of IceCube deployed this year, called the IceCube Upgrade [6]. This is done to show the feasibility for IceCube-Gen2.

## 2. Working principle of the co-deployed laser dust-logger

The LOMlogger needs, similar to the ‘dust logger’, an emitting light source and a receiving photon detector. In the case of the LOMlogger, a modified POCAM [7] and the lowest detector module on the instrumentation cable are used. We call this concept co-deployed. Using parts that will have a purpose beyond the stratigraphy measurement on the instrumentation cable makes the operation more cost efficient and less time consuming.

The emitted light fans out horizontally in a  $60^\circ$  opening angle into the ice, until it gets scattered by dust particles. The extent in horizontal direction leads to more statistics for the measurement. A low beam divergence in vertical direction determines the resolution of the stratigraphy measurement. The used laser will be operated in a pulsed mode with an LD driver circuit, explained in [7]. The laser light source will be the main focus of the following proceeding.

After the first scattering process, it scatters randomly through the ice and eventually is detected by one of the PMTs in the detector module 2 m above the emitter. In the case of the IceCube Upgrade version, the light is detected by a LOM [8]. The LOM consists of 16 PMTs, which improves the directional reconstruction of the detected photons. The recorded data will be stored per PMT in 6 ms time bins, which corresponds to one data point every 1 mm depth.

In order to shield the LOM from light that scatters through the water column in the deployment borehole, baffles are needed. The black nylon brushes should absorb the light, but let the water pass through it. There are two positions for the baffles: one directly on top of the light source to prevent the light from entering the borehole as soon as possible and one halfway between the two modules to mitigate signal contribution from reflected rays. Another mitigation strategy uses the directionality of LOM PMTs. The PMTs facing the opposite side of the light source will likely collect only scattered photons coming through the ice, whereas the PMTs facing the light source might also collect photons reflected through the borehole.



**Figure 2:** Sketch of the LOMlogger setup with the LOM at the top, a baffle halfway between the two modules and the POCAM at the bottom with another baffle attached on top of its harness.

### 3. Requirements for the optics

The LOMlogger project can learn from the dust logger measurements about its required capabilities. The dust logger data was reanalyzed similar to the approach reported in [9]. The data is also publicly available [10]. Using the dynamic time warping algorithm [11], the different stratigraphy measurements could be compared. Features as described in section 1 could be matched even though appearing at different depths in the different measurements.

It is important to identify which features are needed to still be able to match two measurements. Therefore, the goal is to see which resolution is needed to recreate the original analysis of the depth difference performed by Bay et al. [10] within  $\pm 1$  m. To determine the resolution needed for a reasonable stratigraphy, the available dust logger data (one data point every 2 mm) could be averaged to have one data point every 20 cm before the dynamic time warping algorithm is not able to match features properly. This leads to the conclusion that features with a size of approximately 20 cm are used by the algorithm to match different measurement. Hence, these features need to be visible in the stratigraphy measurements.

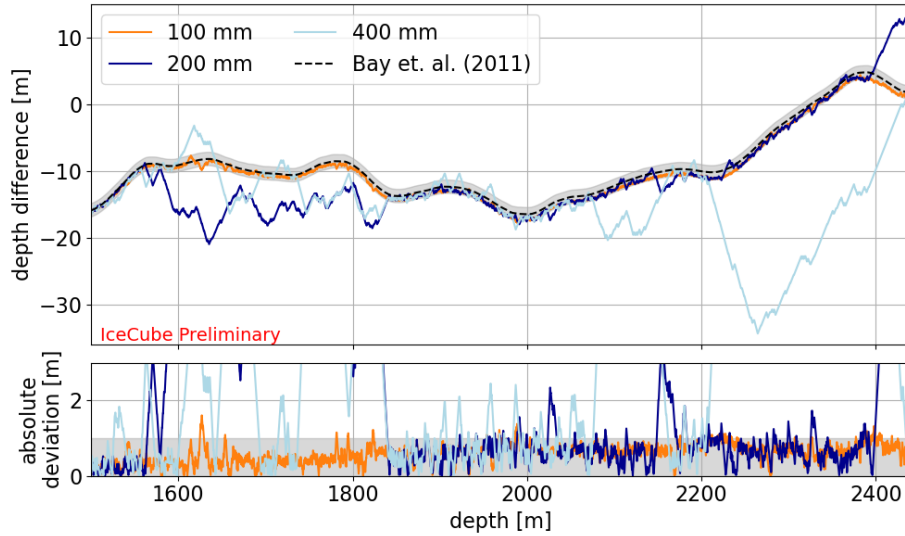
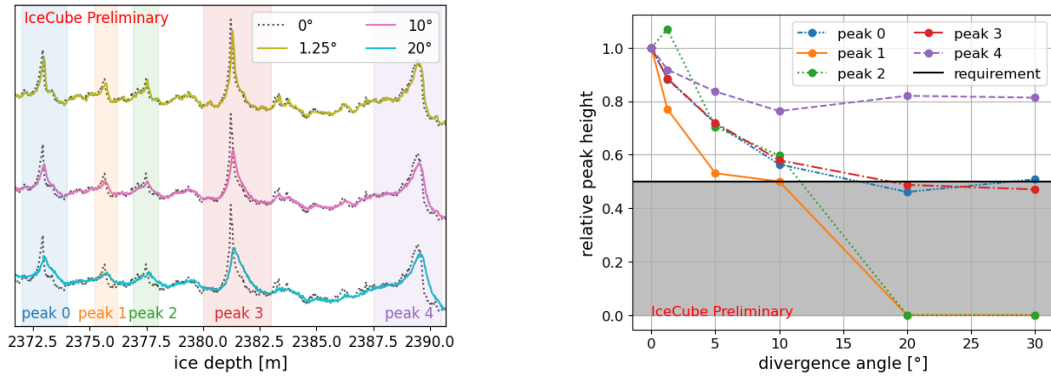


**Figure 3:** Alignment of two stratigraphy measurements over depth with different resolution (see labels in the legend). The black line represents the original analysis [10] and the gray band (representing  $\pm 1$  m) around it is the still allowed region for the fit to diverge from. The lower panel shows the absolute deviation between Bay et al. and this analysis with the different resolutions.

This result was used to find a representative region in the stratigraphy with 5 features of a FWHM of 20 cm (called peaks in Figure 4). Using the PPC simulation tool [12], the LOMlogger was simulated varying the vertical inclination and the beam divergence. The simulation delivers the anticipated stratigraphy where it uses the light source parameters as input. The beam divergence was changed to see when those features would degrade to 50% of the ideal peak height in the stratigraphy simulation. This resulted in a beam divergence that should be less than  $10^\circ$ . Changing the vertical inclination of the beam, shifts the scanned depth area. Hence, the beam inclination should not surpass  $10^\circ$ . These results lead to the incentive to make the beam divergence as small as possible and try to stabilize the device as much as possible during the deployment. The beam



(a) Exemplary stratigraphy simulation with different divergence angle settings for representative features (shaded regions).

(b) Changing divergence angle (x axis) degrades feature visibility shown as relative peak height on the y axis.

**Figure 4:** Simulation of degraded optical systems in a region with 5 representative 20 cm features.

divergence will be discussed later on. The device stability during deployment is mostly out of our hands.

The other important parameter for this operation is the intensity of the laser. It should deliver enough photons that scattered photons reach the receiving LOM, but not enough to saturate it.

The fraction of emitted photons expected to be detected by each PMT was gauged from a PPC [12] photon propagation simulation of the LOMlogger system. In the clearest ice, where the return probability is the lowest, it is  $4.3 \times 10^{-8}$  per LOM PMT. The intensity ratio between the cleanest and the most scattering ice as observed by the old dust logger is 30. So the detection probability per LOM PMT in the most scattering ice is expected to be  $1.3 \times 10^{-6}$ . The LOM PMTs start to saturate at  $\sim 1000$  PE per pulse, assuming a repetition frequency of 1 kHz. So the highest permissible brightness is  $8 \times 10^8$  photons per pulse. To still detect at least 10 photons per pulse in the cleanest ice the light source shall not be dimmer than  $3 \times 10^8$  photons.

#### 4. Optics design

The requirements lead to a few components for the optics system. The complete optics system, including the board that houses the laser is shown in Figure 5. In the following the different parts get described from the bottom (near the PCB) up.

As a light source a 405 nm laser diode (RTL405-600MGE from Roithner) is used. The wavelength was chosen, because ice is the most transparent for 405 nm light [13]. This makes it the most efficient way to transport the light to the detector. The laser diode in particular was chosen, because it was already tested for a similar purpose [14].

The laser beam will be focused by a Thorlabs LTN330-A Adjustable Laser Diode Collimation Tube. The collimation is needed to make the laser as convergent as possible. Testing the prototype this produced an ellipsoid beam profile with FWHM of 0.7 mm and 1.6 mm in x and y direction. This beam profile will be further restricted with a pinhole after the collimator to get the needed beam diameter of 0.4 mm for the beam optics. Beam profiles of the collimated beam and after the pinhole can be found in Figure 6. The 2D-scans are performed by a photodiode on a 2 dimensional

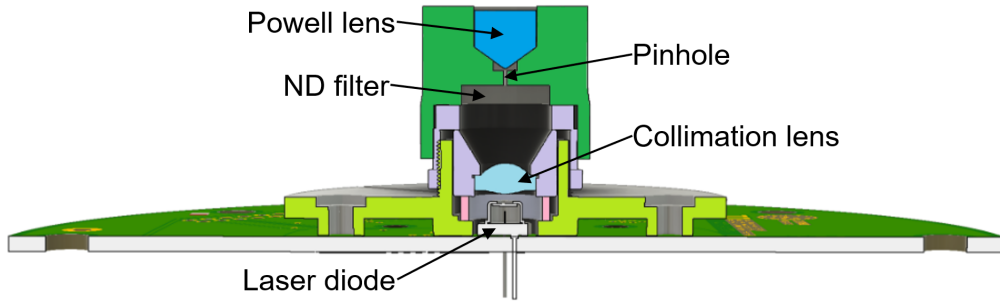


**Figure 5:** CAD model of the LOMlogger optics on the POCAM analog board (bottom part). Sitting directly on the board is the laser (white component) and the 3D-printed collimator holding structure (light green). The 3D-printed part contains parts of the Thorlabs Collimation Tube (spring depicted in pink, lens in light blue and collimation cap in violet). On top sits the 3D-printed Powell lens holding structure (dark green) with integrated cavity for the neutral density filter (gray rectangle), pinhole (small gray bottle neck) and Powell lens (dark blue part).

linear stage. The FWHM was calculated using the one dimensional profile of the beam, by summing up the photodiode output over each column or row. Additionally, a 2D-Gaussian fit was performed as a cross check to get a handle on the beam size.

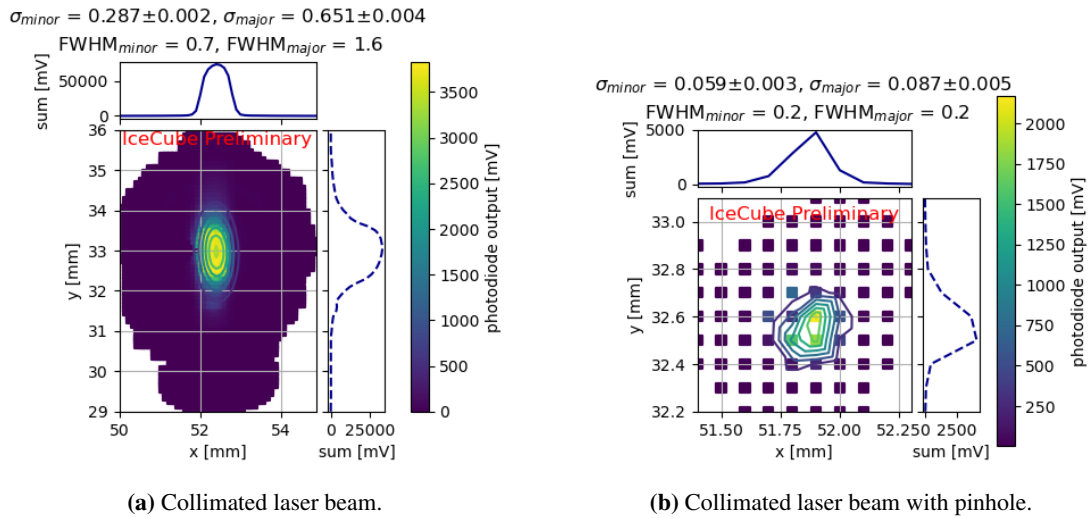


**Figure 6:** 2D-scan of the laser beam profile (lower left panel in the respective plots) with results for FWHM calculation and 2D-Gaussian fit (given on the top). All quantities are given in mm. The right panel in each plot shows the 1D-intensity profile in y-direction and the panel at the top in x-direction.

The requirements showed that a very thin beam in vertical direction is needed. On the other hand the more light shines into the ice in the horizontal direction the more ice in one layer can be probed. Therefore the beam needs to be shaped like a fan. This can be achieved by a LGL160 Powell lens. To produce a even distribution in intensity, the incoming beam needs to have a diameter smaller than 0.4 mm. Hence, the pinhole is placed in front of the lens. A 2D-scan of the final beam going into the ice is shown in Figure 7.

Besides the overall beam profile the divergence of the beam with the Powell lens is important.

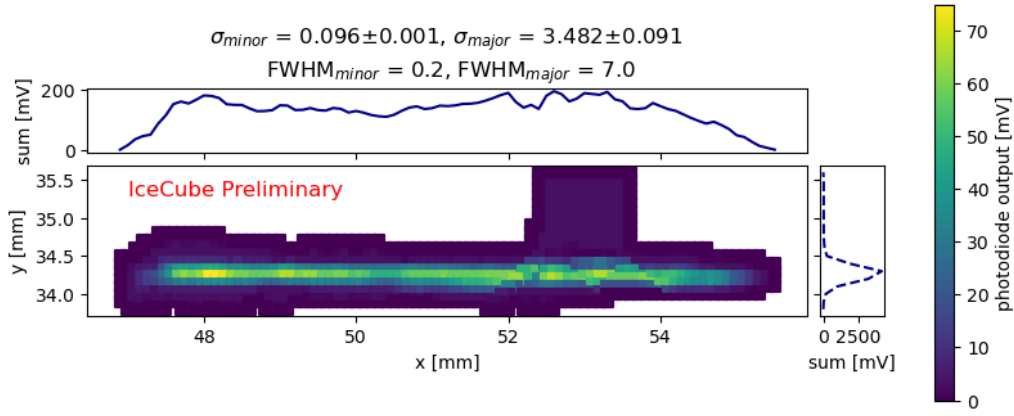


**Figure 7:** 2D-scan of the laser beam profile after the Powell lens was added (lower left panel) with results for FWHM calculation and 2D-Gaussian fit (given on the top). All quantities are given in mm. The right panel in the plot shows the 1D-intensity profile in y-direction and the panel at the top in x-direction.

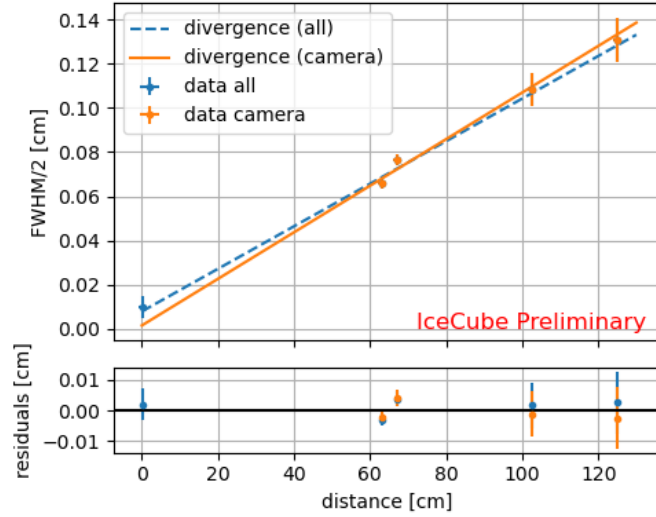


**Figure 8:** Result of the beam divergence measurement. Distance between laser and screen is plotted on the x-axis and half the FWHM is plotted in the upper panel. This is used to perform the linear fit leading to the divergence. The lower panel shows the residuals. The orange dots describe the data taken by the camera method, the blue dot describes the linear stage method.

This was tested with camera pictures taken at different distances between laser and detection screen (fluorescent paper). The divergence angle in y-direction can be calculated using the small angle approximation of the tangent. In this case, a linear fit of distance between laser and screen and half of the FWHM was performed. The result, the slope of the fit, is a divergence angle of  $0.06(1)^\circ$  as shown in Figure 8. As can be seen in the plot the camera method and the linear stage method described above deliver compatible results.

The laser intensity can be reduced with a neutral density filter, if needed. This measure accounts for laser diode intensity variations. The filter can be placed between collimator and pinhole. The reduction of the intensity by a factor of 4 was sufficient in most cases.



## 5. Conclusion

The ice stratigraphy is an important way to improve the neutrino event reconstruction in IceCube. It is the basis for the current ice model and can be improved by further measurements conducted during the deployment of the IceCube Upgrade. It is also important regarding the tilt expected in IceCube-Gen2's larger footprint.

The stratigraphy in the IceCube Upgrade can be measured with a newly developed version of the dust logger using a laser light source (modified POCAM) shining light into the ice while lowering the instrumentation cable into the ice. The light scattered in the ice is detected by one of the photosensor modules (LOM). The two instruments are currently in production and will be deployed this austral summer.

In order to measure the stratigraphy certain requirements for the optics need to be fulfilled. The vertical beam divergence should be less than  $10^\circ$  and also the inclination of the beam should be less than  $10^\circ$  to get a resolution smaller than 20 cm. Additionally, the intensity should be within the range of  $3 \times 10^8 \gamma$  to  $8 \times 10^8 \gamma$  per pulse to surpass the background, but not saturate the LOM.

These requirements lead to a beam design that is very narrow in the vertical direction, but can be broad in the horizontal direction. This can be achieved with a 405 nm laser diode collimated and shaped by a pinhole to an appropriate size for the Powell lens. The Powell lens produces a fan of light with the desired dimensions.

## References

- [1] **IceCube** Collaboration, M. G. Aartsen *et al.*, *JINST* **12** no. 03, (2017) P03012.
- [2] **IceCube** Collaboration, *Journal of Glaciology* **59** no. 218, (2013) 1117–1128.
- [3] **IceCube** Collaboration, D. Chirkin, M. Rongen, *et al.*, *PoS ICRC2023* (2023) 975.
- [4] **IceCube** Collaboration, A. Eimer, M. Rongen, *et al.*, *PoS ICRC2025* (these proceedings) 1035.
- [5] **IceCube-Gen2** Collaboration, M. G. Aartsen *et al.*, *J. Phys. G* **48** no. 6, (2021) 060501.
- [6] **IceCube** Collaboration, A. Ishihara *et al.*, *PoS ICRC2019* (2021) 1031.
- [7] F. Henningsen *et al.*, *Journal of Instrumentation* **15** no. 07, (Jul, 2020) P07031.
- [8] **IceCube** Collaboration, A. Kappes *et al.*, *PoS ICRC2025* (these proceedings) 1072.
- [9] R. C. Bay *et al.*, *Journal of Geophysical Research: Atmospheres* **115** no. D14, (2010) .
- [10] R. Bay, “IceCube dust map.” <http://dustmap.icecube.wisc.edu/>. website.
- [11] C. Myers *et al.*, *IEEE Trans Acoust* **28** no. 6, (1980) 623–635.
- [12] D. Chirkin, *NIM A* **725** (2013) 141–143. VLVNT 2011.
- [13] M. Ackermann *et al.*, *Journal of Geophysical Research: Atmospheres* **111** no. D13, (2006) .
- [14] F. Henningsen, N. Braam, *et al.*, *Journal of Instrumentation* **18** no. 10, (Oct, 2023) P10010.



## Full Author List: IceCube Collaboration

R. Abbasi<sup>16</sup>, M. Ackermann<sup>63</sup>, J. Adams<sup>17</sup>, S. K. Agarwalla<sup>39, a</sup>, J. A. Aguilar<sup>10</sup>, M. Ahlers<sup>21</sup>, J.M. Alameddine<sup>22</sup>, S. Ali<sup>35</sup>, N. M. Amin<sup>43</sup>, K. Andeen<sup>41</sup>, C. Argüelles<sup>13</sup>, Y. Ashida<sup>52</sup>, S. Athanasiadou<sup>63</sup>, S. N. Axani<sup>43</sup>, R. Babu<sup>23</sup>, X. Bai<sup>49</sup>, J. Baines-Holmes<sup>39</sup>, A. Balagopal V.<sup>39, 43</sup>, S. W. Barwick<sup>29</sup>, S. Bash<sup>26</sup>, V. Basu<sup>52</sup>, R. Bay<sup>6</sup>, J. J. Beatty<sup>19, 20</sup>, J. Becker Tjus<sup>9, b</sup>, P. Behrens<sup>1</sup>, J. Beise<sup>61</sup>, C. Bellenghi<sup>26</sup>, B. Benkel<sup>63</sup>, S. BenZvi<sup>51</sup>, D. Berley<sup>18</sup>, E. Bernardini<sup>47, c</sup>, D. Z. Besson<sup>35</sup>, E. Blaufuss<sup>18</sup>, L. Bloom<sup>58</sup>, S. Blot<sup>63</sup>, I. Bodo<sup>39</sup>, F. Bontempo<sup>30</sup>, J. Y. Book Motzkin<sup>13</sup>, C. Boscolo Meneguolo<sup>47, c</sup>, S. Böser<sup>40</sup>, O. Botner<sup>61</sup>, J. Böttcher<sup>1</sup>, J. Braun<sup>39</sup>, B. Brinson<sup>4</sup>, Z. Brisson-Tsouvoussis<sup>32</sup>, R. T. Burley<sup>2</sup>, D. Butterfield<sup>39</sup>, M. A. Campana<sup>48</sup>, K. Carloni<sup>13</sup>, J. Carpio<sup>33, 34</sup>, S. Chattopadhyay<sup>39, a</sup>, N. Chau<sup>10</sup>, Z. Chen<sup>55</sup>, D. Chirkin<sup>39</sup>, S. Choi<sup>52</sup>, B. A. Clark<sup>18</sup>, A. Coleman<sup>61</sup>, P. Coleman<sup>1</sup>, G. H. Collin<sup>14</sup>, D. A. Coloma Borja<sup>47</sup>, A. Connolly<sup>19, 20</sup>, J. M. Conrad<sup>14</sup>, R. Corley<sup>52</sup>, D. F. Cowen<sup>59, 60</sup>, C. De Clercq<sup>11</sup>, J. J. DeLaunay<sup>59</sup>, D. Delgado<sup>13</sup>, T. Delmeulle<sup>10</sup>, S. Deng<sup>1</sup>, P. Desiati<sup>39</sup>, K. D. de Vries<sup>11</sup>, G. de Wasseige<sup>36</sup>, T. DeYoung<sup>23</sup>, J. C. Díaz-Vélez<sup>39</sup>, S. DiKerby<sup>23</sup>, M. Dittmer<sup>42</sup>, A. Domi<sup>25</sup>, L. Draper<sup>52</sup>, L. Dueser<sup>1</sup>, D. Durnford<sup>24</sup>, K. Dutta<sup>40</sup>, M. A. DuVernois<sup>39</sup>, T. Ehrhardt<sup>40</sup>, L. Eidenschink<sup>26</sup>, A. Eimer<sup>25</sup>, P. Eller<sup>26</sup>, E. Ellinger<sup>62</sup>, D. Elsässer<sup>22</sup>, R. Engel<sup>30, 31</sup>, H. Erpenbeck<sup>39</sup>, W. Esmail<sup>42</sup>, S. Eulig<sup>13</sup>, J. Evans<sup>18</sup>, P. A. Evenson<sup>43</sup>, K. L. Fan<sup>18</sup>, K. Fang<sup>39</sup>, K. Farrag<sup>15</sup>, A. R. Fazely<sup>5</sup>, A. Fedynitch<sup>57</sup>, N. Feigl<sup>8</sup>, C. Finley<sup>54</sup>, L. Fischer<sup>63</sup>, D. Fox<sup>59</sup>, A. Franckowiak<sup>9</sup>, S. Fukami<sup>63</sup>, P. Fürst<sup>1</sup>, J. Gallagher<sup>38</sup>, E. Ganster<sup>1</sup>, A. Garcia<sup>13</sup>, M. Garcia<sup>43</sup>, G. Garg<sup>39, a</sup>, E. Genton<sup>13, 36</sup>, L. Gerhardt<sup>7</sup>, A. Ghadimi<sup>58</sup>, C. Glaser<sup>61</sup>, T. Glüsenkamp<sup>61</sup>, J. G. Gonzalez<sup>43</sup>, S. Goswami<sup>33, 34</sup>, A. Granados<sup>23</sup>, D. Grant<sup>12</sup>, S. J. Gray<sup>18</sup>, S. Griffin<sup>39</sup>, S. Griswold<sup>51</sup>, K. M. Groth<sup>21</sup>, D. Guevel<sup>39</sup>, C. Günther<sup>1</sup>, P. Gutjahr<sup>22</sup>, C. Ha<sup>53</sup>, C. Haack<sup>25</sup>, A. Hallgren<sup>61</sup>, L. Halve<sup>1</sup>, F. Halzen<sup>39</sup>, L. Hamacher<sup>1</sup>, M. Ha Minh<sup>26</sup>, M. Handt<sup>1</sup>, K. Hanson<sup>39</sup>, J. Hardin<sup>14</sup>, A. A. Harnisch<sup>23</sup>, P. Hatch<sup>32</sup>, A. Haungs<sup>30</sup>, J. Häußler<sup>1</sup>, K. Helbing<sup>62</sup>, J. Hellrung<sup>9</sup>, B. Henke<sup>23</sup>, L. Hennig<sup>25</sup>, F. Henningsen<sup>12</sup>, L. Heuermann<sup>1</sup>, R. Hewett<sup>17</sup>, N. Heyer<sup>61</sup>, S. Hickford<sup>62</sup>, A. Hidvegi<sup>54</sup>, C. Hill<sup>15</sup>, G. C. Hill<sup>2</sup>, R. Hmaid<sup>15</sup>, K. D. Hoffman<sup>18</sup>, D. Hooper<sup>39</sup>, S. Hori<sup>39</sup>, K. Hoshina<sup>39, d</sup>, M. Hostert<sup>13</sup>, W. Hou<sup>30</sup>, T. Huber<sup>30</sup>, K. Hultqvist<sup>54</sup>, K. Hymon<sup>22, 57</sup>, A. Ishihara<sup>15</sup>, W. Iwakiri<sup>15</sup>, M. Jacquart<sup>21</sup>, S. Jain<sup>39</sup>, O. Janik<sup>25</sup>, M. Jansson<sup>36</sup>, M. Jeong<sup>52</sup>, M. Jin<sup>13</sup>, N. Kamp<sup>13</sup>, D. Kang<sup>30</sup>, W. Kang<sup>48</sup>, X. Kang<sup>48</sup>, A. Kappes<sup>42</sup>, L. Kardum<sup>22</sup>, T. Karg<sup>63</sup>, M. Karl<sup>26</sup>, A. Karle<sup>39</sup>, A. Katil<sup>24</sup>, M. Kauer<sup>39</sup>, J. L. Kelley<sup>39</sup>, M. Khanal<sup>52</sup>, A. Khatee Zathul<sup>39</sup>, A. Kheirandish<sup>33, 34</sup>, H. Kimku<sup>53</sup>, J. Kiryluk<sup>55</sup>, C. Klein<sup>25</sup>, S. R. Klein<sup>6, 7</sup>, Y. Kobayashi<sup>15</sup>, A. Kochocki<sup>23</sup>, R. Koirala<sup>43</sup>, H. Kolanoski<sup>8</sup>, T. Kontrimas<sup>26</sup>, L. Köpke<sup>40</sup>, C. Kopper<sup>25</sup>, D. J. Koskinen<sup>21</sup>, P. Koundal<sup>43</sup>, M. Kowalski<sup>8, 63</sup>, T. Kozynets<sup>21</sup>, N. Krieger<sup>9</sup>, J. Krishnamoorthi<sup>39, a</sup>, T. Krishnan<sup>13</sup>, K. Kruiswijk<sup>36</sup>, E. Krupczak<sup>23</sup>, A. Kumar<sup>63</sup>, E. Kun<sup>9</sup>, N. Kurahashi<sup>48</sup>, N. Lad<sup>63</sup>, C. Lagunas Gualda<sup>26</sup>, L. Lallement Arnaud<sup>10</sup>, M. Lamoureux<sup>36</sup>, M. J. Larson<sup>18</sup>, F. Lauber<sup>62</sup>, J. P. Lazar<sup>36</sup>, K. Leonard DeHolton<sup>60</sup>, A. Leszczyńska<sup>43</sup>, J. Liao<sup>4</sup>, C. Lin<sup>43</sup>, Y. T. Liu<sup>60</sup>, M. Liubarska<sup>24</sup>, C. Love<sup>48</sup>, L. Lu<sup>39</sup>, F. Lucarelli<sup>27</sup>, W. Luszczyk<sup>19, 20</sup>, Y. Lyu<sup>6, 7</sup>, J. Madsen<sup>39</sup>, E. Magnus<sup>11</sup>, K. B. M. Mahn<sup>23</sup>, Y. Makino<sup>39</sup>, E. Manao<sup>26</sup>, S. Mancina<sup>47, e</sup>, A. Mand<sup>39</sup>, I. C. Mariş<sup>10</sup>, S. Marka<sup>45</sup>, Z. Marka<sup>45</sup>, L. Marten<sup>1</sup>, I. Martinez-Soler<sup>13</sup>, R. Maruyama<sup>44</sup>, J. Mauro<sup>36</sup>, F. Mayhew<sup>23</sup>, F. McNally<sup>37</sup>, J. V. Mead<sup>21</sup>, K. Meagher<sup>39</sup>, S. Mechbal<sup>63</sup>, A. Medina<sup>20</sup>, M. Meier<sup>15</sup>, Y. Merckx<sup>11</sup>, L. Merten<sup>9</sup>, J. Mitchell<sup>5</sup>, L. Molchany<sup>49</sup>, T. Montaruli<sup>27</sup>, R. W. Moore<sup>24</sup>, Y. Morii<sup>15</sup>, A. Mosbrugger<sup>25</sup>, M. Moulai<sup>39</sup>, D. Mousadi<sup>63</sup>, E. Moyaux<sup>36</sup>, T. Mukherjee<sup>30</sup>, R. Naab<sup>63</sup>, M. Nakos<sup>39</sup>, U. Naumann<sup>62</sup>, J. Necker<sup>63</sup>, L. Neste<sup>54</sup>, M. Neumann<sup>42</sup>, H. Niederhausen<sup>23</sup>, M. U. Nisa<sup>23</sup>, K. Noda<sup>15</sup>, A. Noell<sup>1</sup>, A. Novikov<sup>43</sup>, A. Obertacke Pollmann<sup>15</sup>, V. O'Dell<sup>39</sup>, A. Olivas<sup>18</sup>, R. Orsoe<sup>26</sup>, J. Osborn<sup>39</sup>, E. O'Sullivan<sup>61</sup>, V. Palusova<sup>40</sup>, H. Pandya<sup>43</sup>, A. Parenti<sup>10</sup>, N. Park<sup>32</sup>, V. Parrish<sup>23</sup>, E. N. Paudel<sup>58</sup>, L. Paul<sup>49</sup>, C. Pérez de los Heros<sup>61</sup>, T. Pernice<sup>63</sup>, J. Peterson<sup>39</sup>, M. Plum<sup>49</sup>, A. Pontén<sup>61</sup>, V. Poojyam<sup>58</sup>, Y. Popovych<sup>40</sup>, M. Prado Rodriguez<sup>39</sup>, B. Pries<sup>23</sup>, R. Procter-Murphy<sup>18</sup>, G. T. Przybylski<sup>7</sup>, L. Pyras<sup>52</sup>, C. Raab<sup>36</sup>, J. Rack-Helleis<sup>40</sup>, N. Rad<sup>63</sup>, M. Ravn<sup>61</sup>, K. Rawlins<sup>3</sup>, Z. Rechav<sup>39</sup>, A. Rehman<sup>39</sup>, I. Reistoffer<sup>49</sup>, E. Resconi<sup>26</sup>, S. Reusch<sup>63</sup>, C. D. Rho<sup>56</sup>, W. Rhode<sup>22</sup>, L. Ricca<sup>36</sup>, B. Riedel<sup>39</sup>, A. Rifaie<sup>62</sup>, E. J. Roberts<sup>2</sup>, S. Robertson<sup>6, 7</sup>, M. Rongen<sup>25</sup>, A. Rosted<sup>15</sup>, C. Rott<sup>52</sup>, T. Ruhe<sup>22</sup>, L. Ruohan<sup>26</sup>, D. Ryckbosch<sup>28</sup>, J. Saffer<sup>31</sup>, D. Salazar-Gallegos<sup>23</sup>, P. Sampathkumar<sup>30</sup>, A. Sandrock<sup>62</sup>, G. Sanger-Johnson<sup>23</sup>, M. Santander<sup>58</sup>, S. Sarkar<sup>46</sup>, J. Savelberg<sup>1</sup>, M. Scarnera<sup>36</sup>, P. Schaile<sup>26</sup>, M. Schaufel<sup>1</sup>, H. Schieler<sup>30</sup>, S. Schindler<sup>25</sup>, L. Schlickmann<sup>40</sup>, B. Schlüter<sup>42</sup>, F. Schlüter<sup>10</sup>, N. Schmeisser<sup>62</sup>, T. Schmidt<sup>18</sup>, F. G. Schröder<sup>30, 43</sup>, L. Schumacher<sup>25</sup>, S. Schwirn<sup>1</sup>, S. Scalfani<sup>18</sup>, D. Seckel<sup>43</sup>, L. Seen<sup>39</sup>, M. Seikh<sup>35</sup>, S. Seunarine<sup>50</sup>, P. A. Seyle Myhr<sup>36</sup>, R. Shah<sup>48</sup>, S. Shefali<sup>31</sup>, N. Shimizu<sup>15</sup>, B. Skrzypek<sup>6</sup>, R. Snihur<sup>39</sup>, J. Soedingrekso<sup>22</sup>, A. Sogaard<sup>21</sup>, D. Soldin<sup>52</sup>, P. Soldin<sup>1</sup>, G. Sommani<sup>9</sup>, C. Spannfellner<sup>26</sup>, G. M. Spiczak<sup>50</sup>, C. Spiering<sup>63</sup>, J. Stachurska<sup>28</sup>, M. Stamatikos<sup>20</sup>, T. Stanev<sup>43</sup>, T. Stezelberger<sup>7</sup>, T. Stürwald<sup>62</sup>, T. Stuttgart<sup>21</sup>, G. W. Sullivan<sup>18</sup>, I. Taboada<sup>4</sup>, S. Ter-Antonyan<sup>5</sup>, A. Terliuk<sup>26</sup>, A. Thakuri<sup>49</sup>, M. Thiesmeyer<sup>39</sup>, W. G. Thompson<sup>13</sup>, J. Thwaites<sup>39</sup>, S. Tilav<sup>43</sup>, K. Tollefson<sup>23</sup>, S. Toscano<sup>10</sup>, D. Tosi<sup>39</sup>, A. Trettin<sup>63</sup>, A. K. Upadhyay<sup>39, a</sup>, K. Upshaw<sup>5</sup>, A. Vaidyanathan<sup>41</sup>, N. Valtonen-Mattila<sup>9, 61</sup>, J. Valverde<sup>41</sup>, J. Vandenbroucke<sup>39</sup>, T. van Eeden<sup>63</sup>, N. van Eijndhoven<sup>11</sup>, L. van Rootselaar<sup>22</sup>, J. van Santen<sup>63</sup>, F. J. Vara Carbonell<sup>42</sup>, F. Varsi<sup>31</sup>, M. Venugopal<sup>30</sup>, M. Vereecken<sup>36</sup>, S. Vergara Carrasco<sup>17</sup>, S. Verpoest<sup>43</sup>, D. Veske<sup>45</sup>, A. Vijai<sup>18</sup>, J. Villarreal<sup>14</sup>, C. Walck<sup>54</sup>, A. Wang<sup>4</sup>, E. Warrick<sup>58</sup>, C. Weaver<sup>23</sup>, P. Weigel<sup>14</sup>, A. Weindl<sup>30</sup>, J. Weldert<sup>40</sup>, A. Y. Wen<sup>13</sup>, C. Wendt<sup>39</sup>, J. Werthebach<sup>22</sup>, M. Weyrauch<sup>30</sup>, N. Whitehorn<sup>23</sup>, C. H. Wiebusch<sup>1</sup>, D. R. Williams<sup>58</sup>, L. Witthaus<sup>22</sup>, M. Wolf<sup>26</sup>, G. Wrede<sup>25</sup>, X. W. Xu<sup>5</sup>, J. P. Yañez<sup>24</sup>, Y. Yao<sup>39</sup>, E. Yildizci<sup>39</sup>, S. Yoshida<sup>15</sup>, R. Young<sup>35</sup>, F. Yu<sup>13</sup>, S. Yu<sup>52</sup>, T. Yuan<sup>39</sup>, A. Zegarelli<sup>9</sup>, S. Zhang<sup>23</sup>, Z. Zhang<sup>55</sup>, P. Zhelnin<sup>13</sup>, P. Zilberman<sup>39</sup>

<sup>1</sup> III. Physikalisches Institut, RWTH Aachen University, D-52056 Aachen, Germany<sup>2</sup> Department of Physics, University of Adelaide, Adelaide, 5005, Australia<sup>3</sup> Dept. of Physics and Astronomy, University of Alaska Anchorage, 3211 Providence Dr., Anchorage, AK 99508, USA<sup>4</sup> School of Physics and Center for Relativistic Astrophysics, Georgia Institute of Technology, Atlanta, GA 30332, USA<sup>5</sup> Dept. of Physics, Southern University, Baton Rouge, LA 70813, USA<sup>6</sup> Dept. of Physics, University of California, Berkeley, CA 94720, USA<sup>7</sup> Lawrence Berkeley National Laboratory, Berkeley, CA 94720, USA<sup>8</sup> Institut für Physik, Humboldt-Universität zu Berlin, D-12489 Berlin, Germany<sup>9</sup> Fakultät für Physik & Astronomie, Ruhr-Universität Bochum, D-44780 Bochum, Germany<sup>10</sup> Université Libre de Bruxelles, Science Faculty CP230, B-1050 Brussels, Belgium

- <sup>11</sup> Vrije Universiteit Brussel (VUB), Dienst ELEM, B-1050 Brussels, Belgium
- <sup>12</sup> Dept. of Physics, Simon Fraser University, Burnaby, BC V5A 1S6, Canada
- <sup>13</sup> Department of Physics and Laboratory for Particle Physics and Cosmology, Harvard University, Cambridge, MA 02138, USA
- <sup>14</sup> Dept. of Physics, Massachusetts Institute of Technology, Cambridge, MA 02139, USA
- <sup>15</sup> Dept. of Physics and The International Center for Hadron Astrophysics, Chiba University, Chiba 263-8522, Japan
- <sup>16</sup> Department of Physics, Loyola University Chicago, Chicago, IL 60660, USA
- <sup>17</sup> Dept. of Physics and Astronomy, University of Canterbury, Private Bag 4800, Christchurch, New Zealand
- <sup>18</sup> Dept. of Physics, University of Maryland, College Park, MD 20742, USA
- <sup>19</sup> Dept. of Astronomy, Ohio State University, Columbus, OH 43210, USA
- <sup>20</sup> Dept. of Physics and Center for Cosmology and Astro-Particle Physics, Ohio State University, Columbus, OH 43210, USA
- <sup>21</sup> Niels Bohr Institute, University of Copenhagen, DK-2100 Copenhagen, Denmark
- <sup>22</sup> Dept. of Physics, TU Dortmund University, D-44221 Dortmund, Germany
- <sup>23</sup> Dept. of Physics and Astronomy, Michigan State University, East Lansing, MI 48824, USA
- <sup>24</sup> Dept. of Physics, University of Alberta, Edmonton, Alberta, T6G 2E1, Canada
- <sup>25</sup> Erlangen Centre for Astroparticle Physics, Friedrich-Alexander-Universität Erlangen-Nürnberg, D-91058 Erlangen, Germany
- <sup>26</sup> Physik-department, Technische Universität München, D-85748 Garching, Germany
- <sup>27</sup> Département de physique nucléaire et corpusculaire, Université de Genève, CH-1211 Genève, Switzerland
- <sup>28</sup> Dept. of Physics and Astronomy, University of Gent, B-9000 Gent, Belgium
- <sup>29</sup> Dept. of Physics and Astronomy, University of California, Irvine, CA 92697, USA
- <sup>30</sup> Karlsruhe Institute of Technology, Institute for Astroparticle Physics, D-76021 Karlsruhe, Germany
- <sup>31</sup> Karlsruhe Institute of Technology, Institute of Experimental Particle Physics, D-76021 Karlsruhe, Germany
- <sup>32</sup> Dept. of Physics, Engineering Physics, and Astronomy, Queen's University, Kingston, ON K7L 3N6, Canada
- <sup>33</sup> Department of Physics & Astronomy, University of Nevada, Las Vegas, NV 89154, USA
- <sup>34</sup> Nevada Center for Astrophysics, University of Nevada, Las Vegas, NV 89154, USA
- <sup>35</sup> Dept. of Physics and Astronomy, University of Kansas, Lawrence, KS 66045, USA
- <sup>36</sup> Centre for Cosmology, Particle Physics and Phenomenology - CP3, Université catholique de Louvain, Louvain-la-Neuve, Belgium
- <sup>37</sup> Department of Physics, Mercer University, Macon, GA 31207-0001, USA
- <sup>38</sup> Dept. of Astronomy, University of Wisconsin—Madison, Madison, WI 53706, USA
- <sup>39</sup> Dept. of Physics and Wisconsin IceCube Particle Astrophysics Center, University of Wisconsin—Madison, Madison, WI 53706, USA
- <sup>40</sup> Institute of Physics, University of Mainz, Staudinger Weg 7, D-55099 Mainz, Germany
- <sup>41</sup> Department of Physics, Marquette University, Milwaukee, WI 53201, USA
- <sup>42</sup> Institut für Kernphysik, Universität Münster, D-48149 Münster, Germany
- <sup>43</sup> Bartol Research Institute and Dept. of Physics and Astronomy, University of Delaware, Newark, DE 19716, USA
- <sup>44</sup> Dept. of Physics, Yale University, New Haven, CT 06520, USA
- <sup>45</sup> Columbia Astrophysics and Nevis Laboratories, Columbia University, New York, NY 10027, USA
- <sup>46</sup> Dept. of Physics, University of Oxford, Parks Road, Oxford OX1 3PU, United Kingdom
- <sup>47</sup> Dipartimento di Fisica e Astronomia Galileo Galilei, Università Degli Studi di Padova, I-35122 Padova PD, Italy
- <sup>48</sup> Dept. of Physics, Drexel University, 3141 Chestnut Street, Philadelphia, PA 19104, USA
- <sup>49</sup> Physics Department, South Dakota School of Mines and Technology, Rapid City, SD 57701, USA
- <sup>50</sup> Dept. of Physics, University of Wisconsin, River Falls, WI 54022, USA
- <sup>51</sup> Dept. of Physics and Astronomy, University of Rochester, Rochester, NY 14627, USA
- <sup>52</sup> Department of Physics and Astronomy, University of Utah, Salt Lake City, UT 84112, USA
- <sup>53</sup> Dept. of Physics, Chung-Ang University, Seoul 06974, Republic of Korea
- <sup>54</sup> Oskar Klein Centre and Dept. of Physics, Stockholm University, SE-10691 Stockholm, Sweden
- <sup>55</sup> Dept. of Physics and Astronomy, Stony Brook University, Stony Brook, NY 11794-3800, USA
- <sup>56</sup> Dept. of Physics, Sungkyunkwan University, Suwon 16419, Republic of Korea
- <sup>57</sup> Institute of Physics, Academia Sinica, Taipei, 11529, Taiwan
- <sup>58</sup> Dept. of Physics and Astronomy, University of Alabama, Tuscaloosa, AL 35487, USA
- <sup>59</sup> Dept. of Astronomy and Astrophysics, Pennsylvania State University, University Park, PA 16802, USA
- <sup>60</sup> Dept. of Physics, Pennsylvania State University, University Park, PA 16802, USA
- <sup>61</sup> Dept. of Physics and Astronomy, Uppsala University, Box 516, SE-75120 Uppsala, Sweden
- <sup>62</sup> Dept. of Physics, University of Wuppertal, D-42119 Wuppertal, Germany
- <sup>63</sup> Deutsches Elektronen-Synchrotron DESY, Platanenallee 6, D-15738 Zeuthen, Germany
- <sup>a</sup> also at Institute of Physics, Sachivalaya Marg, Sainik School Post, Bhubaneswar 751005, India
- <sup>b</sup> also at Department of Space, Earth and Environment, Chalmers University of Technology, 412 96 Gothenburg, Sweden
- <sup>c</sup> also at INFN Padova, I-35131 Padova, Italy
- <sup>d</sup> also at Earthquake Research Institute, University of Tokyo, Bunkyo, Tokyo 113-0032, Japan
- <sup>e</sup> now at INFN Padova, I-35131 Padova, Italy

## **Acknowledgments**

The authors gratefully acknowledge the support from the following agencies and institutions: USA – U.S. National Science Foundation-Office of Polar Programs, U.S. National Science Foundation-Physics Division, U.S. National Science Foundation-EPSCoR, U.S. National Science Foundation-Office of Advanced Cyberinfrastructure, Wisconsin Alumni Research Foundation, Center for High Throughput Computing (CHTC) at the University of Wisconsin–Madison, Open Science Grid (OSG), Partnership to Advance Throughput Computing (PATH), Advanced Cyberinfrastructure Coordination Ecosystem: Services & Support (ACCESS), Frontera and Ranch computing project at the Texas Advanced Computing Center, U.S. Department of Energy-National Energy Research Scientific Computing Center, Particle astrophysics research computing center at the University of Maryland, Institute for Cyber-Enabled Research at Michigan State University, Astroparticle physics computational facility at Marquette University, NVIDIA Corporation, and Google Cloud Platform; Belgium – Funds for Scientific Research (FRS-FNRS and FWO), FWO Odysseus and Big Science programmes, and Belgian Federal Science Policy Office (Belspo); Germany – Bundesministerium für Forschung, Technologie und Raumfahrt (BMFT), Deutsche Forschungsgemeinschaft (DFG), Helmholtz Alliance for Astroparticle Physics (HAP), Initiative and Networking Fund of the Helmholtz Association, Deutsches Elektronen Synchrotron (DESY), and High Performance Computing cluster of the RWTH Aachen; Sweden – Swedish Research Council, Swedish Polar Research Secretariat, Swedish National Infrastructure for Computing (SNIC), and Knut and Alice Wallenberg Foundation; European Union – EGI Advanced Computing for research; Australia – Australian Research Council; Canada – Natural Sciences and Engineering Research Council of Canada, Calcul Québec, Compute Ontario, Canada Foundation for Innovation, WestGrid, and Digital Research Alliance of Canada; Denmark – Villum Fonden, Carlsberg Foundation, and European Commission; New Zealand – Marsden Fund; Japan – Japan Society for Promotion of Science (JSPS) and Institute for Global Prominent Research (IGPR) of Chiba University; Korea – National Research Foundation of Korea (NRF); Switzerland – Swiss National Science Foundation (SNSF).